The Scientific Journal of University of Benghazi

SJUOB (2024) 37 (1) Applied Sciences: 65 – 80

Etaig et al

http://journals.uob.edu.ly/sjuob

Selecting the Optimal Airfoil for Automotive Rear Wings: Performance Assessment

Osama Maddani [1] - Saleh Etaig [1*] - Al-Hadi Ebrahim - [1] Islam AlJhani [1]

1 Mechanical Engineering department - Faculty of Engineering - University of Benghazi.

Received: 22 / 03 / 2024; Accepted: 15 / 05 / 2024

ABSTRACT

This study investigates the potential performance and safety improvements achievable through the application of inverted airfoils on a BMW 3-series (E36) car. Computational fluid dynamics (CFD) simulations were employed to assess the aerodynamic characteristics of three distinct airfoil designs: NACA 0012, NACA 4412, and Eppler E423. Evaluations were conducted at 0°in freestream and at 14° angles of attack (AOA) when used in the automotive application to analyze the impact on lift and drag forces. The findings revealed unique aerodynamic profiles for each airfoil. The angle of attack for the airfoils in freestream was chosen to be 0 degrees to isolate the effect of the different airfoil shapes on their performance. This allows us to better understand how their performance translates to the automotive application. Considering automotive applications, the Eppler E423 demonstrated superior potential for enhanced acceleration and cornering speeds compared to the other airfoils. The NACA 4412 also displayed comparable performance to the Eppler E423 in these aspects. Overall, the inclusion of an Eppler E423 airfoil positioned as an inverted wing at a 14° AOA emerged as the configuration offering the optimal balance between performance and safety benefits for the BMW 3-series (E36). This research underscores the significant potential of strategically incorporating aerodynamic devices, such as inverted wings, to achieve improvements in both vehicle safety and performance characteristics.

KEYWORDS: Automotive aerodynamics, Numerical simulation, Airfoil, Turbulence models.

1. INTRODUCTION

In recent years, automotive aerodynamics has garnered significant attention within the industry, largely driven by increased awareness of fuel consumption. The streamlined shapes of vehicles play a crucial role, as less aerodynamic resistance force, commonly known as drag, is generated. Consequently, overcoming this drag necessitates more engine power, ultimately leading to higher fuel consumption. Moreover, the escalating speeds attained by both sports road vehicles and motorsport racing cars accentuate the need for enhanced stability. Achieving this stability typically involves balancing the lift forces acting on the vehicle's body, among other factors.

Several studies have investigated the use of CFD for airfoil analysis and selection, demonstrating the effectiveness of different turbulence models and highlighting key considerations for unmanned aerial vehicles (UAVs)

*__Correspondence__: Saleh Etaig

Saleh.Etaig@uob.edu.ly

Douvi et al [1] achieved the most accurate results for the NACA 0012 airfoil when using the Spalart-Allmaras turbulence model, compared to k-ε and SST k-ω models. Their study emphasizes the importance of rigorous model validation for reliable outcomes.

Kevadiya and Vaidya [2] obtained good results for the NACA 4412 airfoil using Spalart-Allmaras. Their work focused on a lower angle of attack range (0°-12°) compared to Douvi et al [1].

Reza et al [3] conducted a comprehensive analysis of various airfoils for high-lift, low-Re UAVs. They initially evaluated EPPLER, SELIG, WORTMANN, AG35, and NLF 0115 airfoils. Further analysis based on drag polar at a standard Re for low-speed UAVs led them to select E420, E423, FX74-CL5-140, and S1223 for further scrutiny. Ultimately, S1223 emerged as the most suitable option due to its superior C_l and C_m characteristics and slightly higher stall angle compared to E420.

Parhcal[4] computationally modeled a NACA 4412 airfoil as both front and rear wings for a racing vehicle, aiming to increase downforce and enhance stability. His study analyzed the ground effect, varying angles of attack, and optimized configurations for maximum downforce and minimum drag, finding potential design parameters.

 ISSN:Online 2790-1637, Print 2790-1629; National Library of Libya, Legal number : 154/2018

Ahmad et al [5] validated 2D flow simulations of a NACA 0012 airfoil using the k-ω SST turbulence model, comparing against experimental data from Theory of Wing Sections [6], Employing this validated technique, they analyzed a plain flapped NACA 0012 airfoil at varying flap angles revealing that drag coefficients (CD) remain relatively constant.

Abobaker et al [6] numerically investigated the impact of wind tunnel walls on airfoil measurements, specifically focusing on the lift curve slope correction factor (Ka). They analyzed subsonic flow over a NACA 0012 airfoil at varying angles of attack and domain heights using CFD with SST-Kω turbulence modeling. Their numerical results, validated against experimental data, demonstrate the importance of CFD in understanding and correcting for wind tunnel wall effects.

In their study, Dinesh Bhatia et al [7] conducted simulations of a 2D NACA 0012 airfoil. They highlighted that positioning the sharkskin denticles at 0.16 of the airfoil's chord length in the normal direction resulted in a maximum drag reduction of 3% and an enhancement in lift-to-drag ratio (L/D) of 1.5%. These optimal improvements were observed at angles of attack (AOA) of 0° and 4°. Several efforts focused on studying turbulence models such as [8]

In a separate investigation focusing on modifications of the NACA 0012 airfoil, Sogukpinar [9] explored the impact of varying thicknesses on the lower surface of the airfoil. The resultant data were then compared with observational data from NASA[11,12] to validate the accuracy of the computational approach.

Karim et al [10] investigated the behavior of a hydrofoil submerged in water, focusing on the influence of the water surface boundary position. Their study involved 2D simulations of a NACA 0015 hydrofoil, with an angle of attack (AOA) of 5°. The realizable k-ε turbulence model was employed for turbulence modeling.

Azim et al[11] determined that implementing a suction slot modification effectively delayed separation in a NACA 4412 airfoil operating at Mach number 0.6 and an angle of attack (AOA) of 12°. They utilized the Spalart-Allmaras turbulence model. Consequently, the lift-to-drag ratio (C_l/C_d) increased approximately 2.24 times compared to the airfoil without suction.

Hossain et al [12] concluded that for practical applications, the NACA 4412 airfoil outperforms the NACA 6409. Their comparison was based on the results of coefficient of drag (C_d) and coefficient of lift (C_l) obtained under identical boundary conditions, specifically at angles of attack (AOA) of 0° and 5°.

Singh et al [13] conducted a comparison study indicating that the NACA 4412 airfoil is well-suited for sports planes, whereas the S1223 airfoil is more appropriate for heavy lift cargo planes. Their simulations were carried out within an angle of attack (AOA) range of 0° to 10°.

Amit Saraf et al conducted investigations on the NACA 4412 airfoil in 2D, as detailed in their studies[14] and [15] Their findings suggest that turbulence models namely the standard k-ε, k-ω, and Spalart-Allmaras models, do not yield accurate results at high angles of attack (AOA). The simulations were conducted at a flow velocity of 50 m/s, spanning an AOA range of 0° to 15.

Petinrin and Onoja [16] investigated the accuracy of turbulence models, particularly focusing on the NACA 4412 airfoil. Their study revealed that the SST k-ω transport turbulence model demonstrates superior accuracy compared to the Spalart-Allmaras model. Additionally, the authors observed that the increase in aerodynamic performance of the airfoil diminishes exponentially with increasing Reynolds numbers.

Wina and Thian wiboon [17] conducted a comprehensive investigation using 2D simulations of the NACA 4412 airfoil, exploring variations in angles of attack (AOA). Their study covered an AOA range of 4° to 8° in ground effect in three height to chord length (H/C) ratios 0.1, 0.15 and 0.2. They concluded that as the H/C decreases, the coefficient of lift (C_l) increases and the coefficient of drag (C_d) decreases, leading to a higher lift-to-drag ratio in ground effect.

Ockfen and Matveev [18] presented a study on the NACA 4412 airfoil, focusing on small angles of attack (AOA). They observed that the coefficient of lift (Cl) increases across all ground heights. However, they noticed a significant increase in the coefficient of drag (Cd) as the flap is deflected.

Qiulin Qu et al [19] investigated the influence of Dynamic Ground Effect (DGE) on the NACA 4412 airfoil through 2D simulations. They conducted simulations at an angle of attack of α=3.6°. To validate their simulations, they computed the flow past the Tyrrell-026 airfoil and compared the results with experimental data.

Huminic and Huminic [20] investigated the E423 airfoil and discovered that the Coandă effect, achieved through a curved slot in the underside of the airfoil located at 0.6 of the Chord and has a width of 0.7 mm and a curve radius of 5mm. This improvement enhanced the aerodynamic characteristics of the ailerons, ultimately leading to an enhancement in the aerodynamic behavior of the vehicle in terms of aerodynamic loads. Their study conducted at an angle of attack (AOA) range of 0° to 10°.

Omkar Bhatkar et al [21] conducted a study on a modified version of the E423 airfoil and its impact on vehicle aerodynamics. They found that the generation of downforce substantially affect race car performance. The study focused on the NACA's E423 multi-elemental

 ISSN:Online 2790-1637, Print 2790-1629; National Library of Libya, Legal number : 154/2018

airfoil's front wing and rear wing. Their results indicated a coefficient of lift (C_l) of -1.37 for the front wing and -1.48 for the rear wing.

Sreejith and Sathyabhama [22], conducted a study on the E216 airfoil, where they found that the implementation of a boundary layer trip could partially or completely eliminate the laminar separation bubble (LSB), thereby enhancing the aerodynamic performance of the airfoil. They observed that the maximum improvement in drag reached 15.48%, while the lift-to-drag ratio improved by 21.62% at an angle of attack (AOA) of 6° across all cases.

Guda et al [23] found that employing a double spoiler design, featuring both upper and lower spoilers, effectively reduced the coefficient of drag (C_d) from 0.34 to 0.3 in a Maruti 800 car model. To ensure the accuracy of their findings, the authors validated their simulations against the actual model provided by the manufacturer.

Kumar et al [24] determined that among three spoilers added to a sedan car, the second spoiler yielded the most favorable results. They achieved a coefficient of drag (C_d) of approximately 0.329 and a coefficient of lift (C_l) of 0.106. The authors concluded that the addition of the spoiler resulted in a reduction in the coefficient of drag compared to the baseline configuration.

From the above explored survey of the literature, it can be concluded that there is a gap in studying various airfoils configurations in terms of performance as well as its impact in a rear wing car especially when it comes to an actual vehicle, hence the main contribution of the present study is focused on developing a numerical model and validating it to accurately predict the aerodynamic behavior of various bodies in freestream conditions, enhancing understanding of their performance characteristics.

The performance is thoroughly investigated by exploration of selected airfoils using diverse turbulence models, leading to a comprehensive analysis of their aerodynamic features and behaviors in freestream environments. The study comprises comparison of simulated results with experimental data, facilitating the validation process and strengthening the credibility of the numerical simulations. In addition, a detailed examination of the BMW 3-series (E36) both in its original, wingless state and with the addition of various inverted wings (Airfoils) is presented, shedding light on their respective aerodynamic properties and effectiveness.

2. NUMERICAL METHOD

The present work was conducted using CFD which is a robust tool to investigate and analyze sophisticated fluid flow cases. The governing equations, turbulence model and mesh test will be discussed in detail.

Governing equations

The governing equations are: continuity equations which can be written as:

$$\frac{\partial \rho}{\partial t} + \left(\frac{\partial \rho u}{\partial x} + \frac{\partial \rho v}{\partial y} + \frac{\partial \rho w}{\partial z}\right) = 0 \quad (1)$$

The momentum equation which can be written as:

$$\rho \frac{dV}{dt} = \rho g - \nabla P + \nabla \tau_{ij} \ (2)$$

The Navier stokes equations can be expressed in x, y and z directions as:

X- Momentum

$$\frac{\partial(\rho u)}{\partial t} + \frac{\partial(\rho u^2)}{\partial x} + \frac{\partial(\rho uv)}{\partial y} + \frac{\partial(\rho uw)}{\partial z} = -\frac{\partial p}{\partial x} + \frac{\partial}{\partial x}\left(\lambda \nabla . \mathbf{V} + 2\mu \frac{\partial u}{\partial x}\right) + \frac{\partial}{\partial y}\left[\mu\left(\frac{\partial v}{\partial x} + \frac{\partial u}{\partial y}\right)\right] + \frac{\partial}{\partial z}\left[\mu\left(\frac{\partial u}{\partial z} + \frac{\partial w}{\partial x}\right)\right] + \rho f_x \quad (3)$$

Y-Momentum

$$\frac{\partial(\rho v)}{\partial t} + \frac{\partial(\rho uv)}{\partial x} + \frac{\partial(\rho v^2)}{\partial y} + \frac{\partial(\rho vw)}{\partial z} = -\frac{\partial p}{\partial y} + \frac{\partial}{\partial x}\left[\mu\left(\frac{\partial v}{\partial x} + \frac{\partial u}{\partial y}\right)\right] + \frac{\partial}{\partial y}\left(\lambda \nabla . \mathbf{V} + 2\mu \frac{\partial v}{\partial y}\right) + \frac{\partial}{\partial z}\left[\mu\left(\frac{\partial w}{\partial y} + \frac{\partial v}{\partial z}\right)\right] + \rho f_y \quad (4)$$

Z-Momentum

$$\frac{\partial(\rho w)}{\partial t} + \frac{\partial(\rho uw)}{\partial x} + \frac{\partial(\rho vw)}{\partial y} + \frac{\partial(\rho w^2)}{\partial z} = -\frac{\partial p}{\partial z} + \frac{\partial}{\partial x}\left[\mu\left(\frac{\partial u}{\partial z} + \frac{\partial w}{\partial x}\right)\right] + \frac{\partial}{\partial y}\left[\mu\left(\frac{\partial w}{\partial y} + \frac{\partial v}{\partial z}\right)\right] + \frac{\partial}{\partial z}\left(\lambda \nabla . \mathbf{V} + 2\mu \frac{\partial w}{\partial z}\right) + \rho f_z \quad (5)$$

Reynolds average Navier stokes equations:

$$\frac{\partial(\bar{\rho}\tilde{U})}{\partial t} + \nabla.\left(\bar{\rho}\tilde{U}\tilde{\mathrm{U}}\right) = -\frac{\partial \bar{P}}{\partial x} + \nabla.\left(\mu \nabla \tilde{U}\right) + \left[-\frac{\partial\left(\overline{\rho u'^2}\right)}{\partial x} - \frac{\partial\left(\overline{\rho u'v'}\right)}{\partial y} - \frac{\partial\left(\overline{\rho u'w'}\right)}{\partial z}\right] + S_{Mx} \quad (6$$

$$\frac{\partial(\bar{\rho}\tilde{U})}{\partial t} + \nabla.\left(\bar{\rho}\tilde{V}\tilde{\mathrm{U}}\right) = -\frac{\partial \bar{P}}{\partial y} + \nabla.\left(\mu \nabla \tilde{V}\right) + \left[-\frac{\partial\left(\overline{\rho u'v'}\right)}{\partial x} - \frac{\partial\left(\overline{\rho v'^2}\right)}{\partial y} - \frac{\partial\left(\overline{\rho v'w'}\right)}{\partial z}\right] + S_{My} \quad (7$$

 ISSN:Online 2790-1637, Print 2790-1629; National Library of Libya, Legal number : 154/2018

$$\frac{\partial(\bar{\rho}\widetilde{U})}{\partial t} + \nabla.(\bar{\rho}\widetilde{W}\widetilde{U}) = -\frac{\partial \bar{P}}{\partial z} + \nabla.(\mu\nabla\widetilde{W}) + \left[-\frac{\partial(\overline{\rho u'v'})}{\partial x} - \frac{\partial(\overline{\rho v'w'})}{\partial y} - \frac{\partial(\overline{\rho w'^2})}{\partial z}\right] + S_{Mw} \quad (8$$

Scalar transport equation:

$$\frac{\partial(\bar{\rho}\tilde{\phi})}{\partial t} + \nabla.(\bar{\rho}\tilde{\phi}\widetilde{U}) = \nabla.\left(\Gamma_{\phi}\nabla\tilde{\phi} + \left[-\frac{\partial(\bar{\rho}\overline{u'\phi'})}{\partial x} - \frac{\partial(\bar{\rho}\overline{v'\phi'})}{\partial y} - \frac{\partial(\bar{\rho}\overline{w'\phi'})}{\partial z}\right] + S_{\phi}\right) \quad (9)$$

The models that were used in the current study are: Spalart-Allmaras (one equation), k-ε (Two equation), $k-\omega$ (Two equation), k-ω SST (two equation), k-kl-ω Transition Model, and Transition SST Model

coefficient of drag (C_d), and the coefficient of lift (C_l) are given by

$$C_d = \frac{D}{\frac{1}{2}\rho V^2 A} \quad (10)$$

$$C_l = \frac{L}{\frac{1}{2}\rho V^2 A} \quad (11)$$

Where D and L are the drag and the lift forces respectively, ρ is the air density, V is the air freestream velocity, and A is the projected area.

Case Geometry:

The airfoil's geometry and mesh were created using ANSYS ICEM CFD software, with a chord length of 1 meter and an angle of attack of 0 degrees. The choice of this angle of attack was chosen to highlight the effect the difference in camber and shape of the airfoil had on its performance, and how this could translate to its performance in the automotive application. A NACA0012 profile was utilized for the mesh test, which was then applied to other airfoils. The fluid domain dimensions are depicted in Figure 1 below:

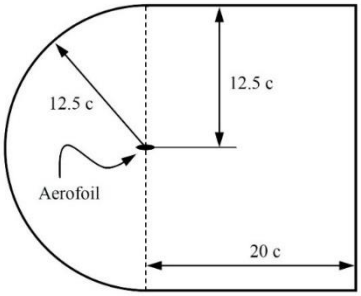

Fig. 1. Airfoil domain dimensions

The mesh was structured in a C-type configuration using blocks, as illustrated in Figure 2, to ensure organized meshing and smooth transition with minimal skewness and element distortion, facilitating a fine mesh. Achieving an accurate solution necessitated very fine mesh elements near the wall, thus a first layer spacing of 8x10^-6 meters was employed, with a growth rate of 1.1

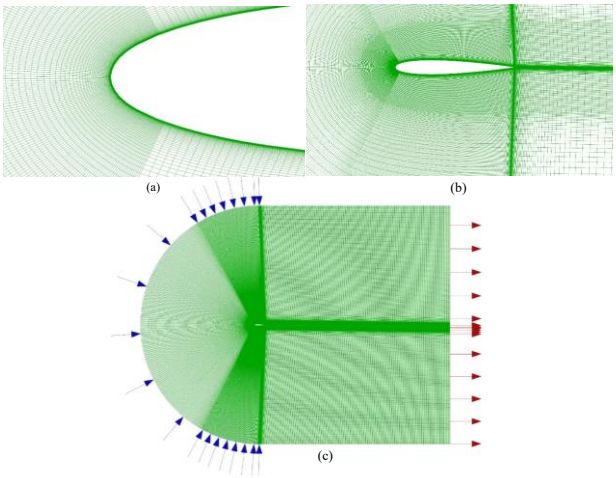

Fig. 2. (a) Airfoil leading edge mesh closeup, (b) Airfoil mesh closeup, (c) Airfoil domain mesh

Car mesh:

The car mesh was generated in 2-D modeled after a BMW 3 series (E36), the dimensions were taken from BMW's service manual, the mesh and geometry were created in ANSYS ICEM CFD as illustrated in Figure 3.

 ISSN:Online 2790-1637, Print 2790-1629; National Library of Libya, Legal number : 154/2018

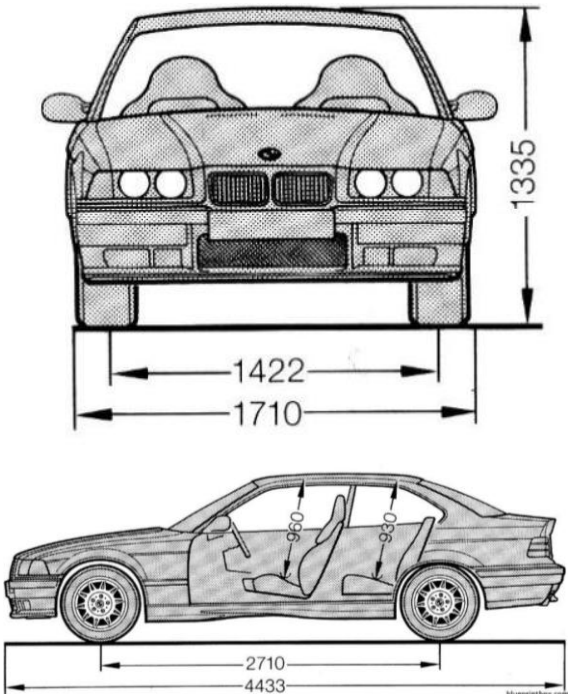

Fig. 3. BMW 3 series (E36) blueprint

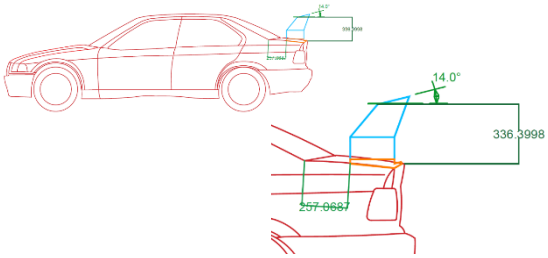

(a)

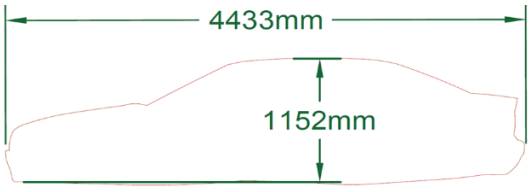

(b)

Fig. 4. (a) BMW 3 series (E36) CAD design of the rear wing, (b) BMW 3 series (E36) 2D drawing of the car body's outline used in the simulation

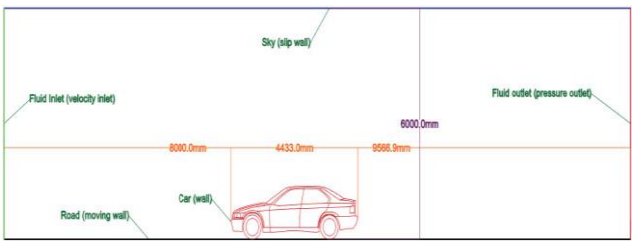

Fig. 5. BMW 3 series (E36) Fluid domain dimensions and boundaries

The mesh was refined by dividing the mesh blocks to avoid skewed elements and to improve quality.The fluid domain which represents the air flowing around the car was drawn as shown in Figure 5.

The boundaries are identified as shown in the Figure 5, sky is assumed a slip wall, the road as a moving wall, the car as wall, fluid inlet as a velocity inlet, and the fluid outlet as a pressure outlet, the airfoil was placed according to the CAD design in the Figure 4, the dimensions were referenced from a real wing used in BMW race cars, measurements were taken to replicate the real wing, although different airfoil sections were used, but all are at 14° AOA relative to the horizontal not the airstream coming down from the car's roof, although the angle could be optimised to avoid separation that may lead to (stall), but this wasn't withing the objective of the current study, Stall is where the streamlines do not follow the airfoil shapes and the flow will be separated. This will result in dramatic loss of lift (stall) and sudden increase in drag, as shown in Figure 6 Below [28].

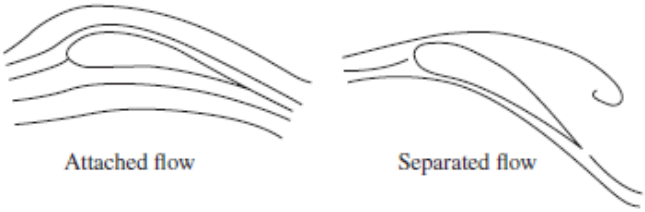

Fig. 6. Schematic description of the streamlines in airfoil attached and separated flow [28]

The airfoil was placed according to the CAD design in the Figure 5(a), the dimensions were referenced from a real wing used in BMW race cars, measurements were taken to replicate the real wing, although different airfoil sections were used, but all are at 14° AOA.

The airfoil (inverted wing was drawn in its specified place) above the rear boot lid, and meshing was made. Figure 7depicts the complete mesh of the fluid domain, blue arrows represent the air entering and red arrows represent the air leaving the domain.

The mesh minimum determinant quality was 0.7, and the minimum angle in the mesh was 18 degrees, the values of these mesh metrics are acceptable according to ICEM CFD's tutorial manual (29) which predicts a reasonable solution.

Mesh test and model validation:

In order to ensure that the solution is independent of the mesh, a mesh test is carried out. Two meshes were generated, one for the simulation of the airfoils, and one for the simulation of the car, which is the application of the present work for the airfoil.

 ISSN:Online 2790-1637, Print 2790-1629; National Library of Libya, Legal number : 154/2018

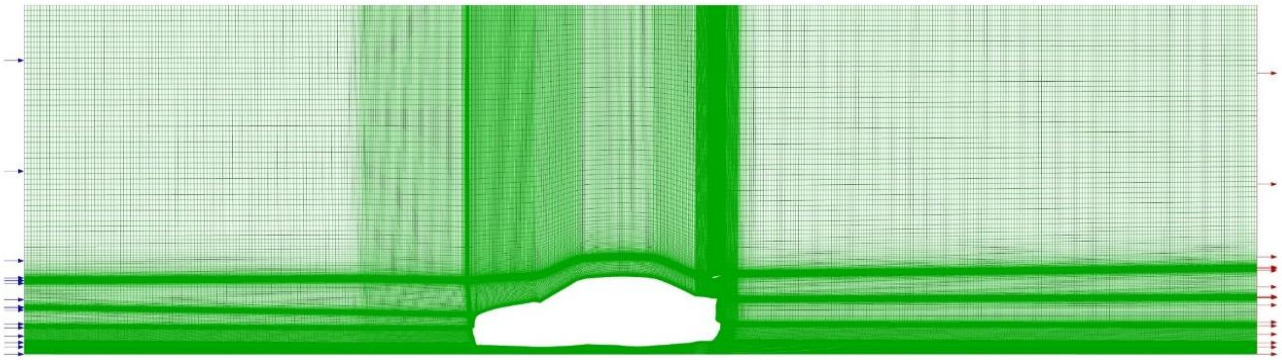

Fig. 7. BMW 3 series (E36) Fluid domain dimensions and boundaries

Several turbulence models were testesd in order to ascertainthesuitability of each model for given conditions

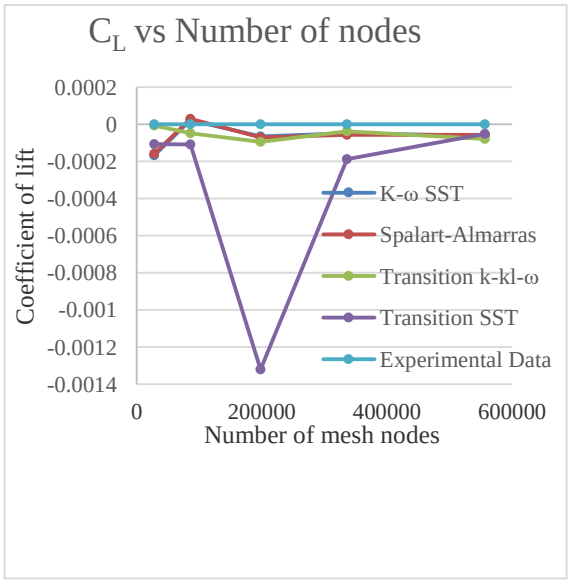

Fig. 8. C_l vs number of nodes

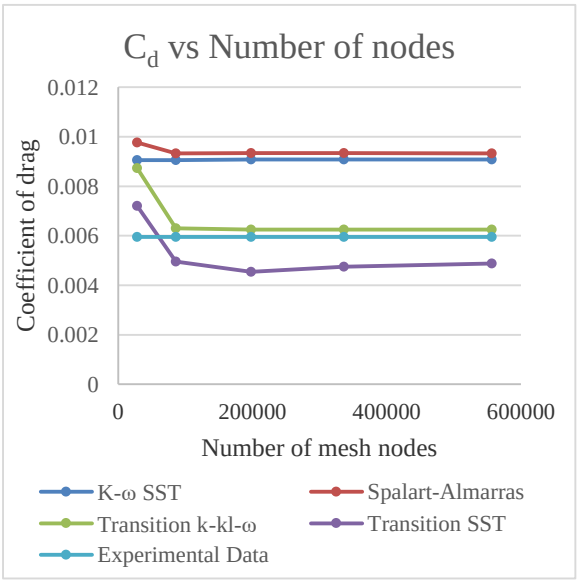

Fig. 9. C_d vs number of nodes

Airfoil mesh test:

The mesh is tested on a NACA0012 airfoil,

 ISSN:Online 2790-1637, Print 2790-1629; National Library of Libya, Legal number : 154/2018

Table 1 NACA0012 mesh sensitivity test

Cd					
[Nodes\model]	**K-ω SST**	**Spalart-Allmaras**	**Transition k-kl-ω**	**Transition SST**	**Experiment Data**
28380	0.009064248	0.009765499	0.008739613	0.00721464	0.00596
85792	0.009061483	0.009330248	0.006297206	0.004964117	
197932	0.009084467	0.009342926	0.006256086	0.004541023	
336124	0.009084229	0.009337151	0.00625686	0.004757129	
556604	0.009079381	0.009330945	0.006254567	0.004882753	
CL					
28380	-0.00016592	-0.00015697	-0.00000627	-0.00010534	0
85792	0.0000235	0.0000299	-0.000047	-0.00010735	
197932	-0.0000648	-0.0000701	-0.0000941	-0.00132037	
336124	-0.0000483	-0.0000562	-0.0000363	-0.00018634	
556604	-0.0000614	-0.0000568	-0.0000783	-0.0000507	

As can be seen from the mesh test graphs at Figure 8 and Figure 9, the most accurate turbulence model for the given conditions is the Transition k-kl-ω, and after 336124 nodes the solution becomes independent of the mesh, the other models show relative independence but they are less accurate, the accuracy of the Transition k-kl-ω model is shown in the C_d results, In terms of C_l, most models demonstrated a reasonable level of accuracy.

The next step is the model validation of the present work, using Eleni Douvi [1] as the validation for the present project, the 80 k nodes mesh was utilizedto compare it to the same cell count as was used in Douvi's study,and compared the same NACA0012 airfoil at the same Re number of $3x10^6$, at an angle of attack of 0°.

Table 2 Airfoil model validation

	CFD current mesh (80k nodes and k-kl-ω)	**Douvi (1)**	**Deviation %**
Cd	0.006370985	0.00635815	0.201 %
Cl	-0.000173073	0	Not Applicable

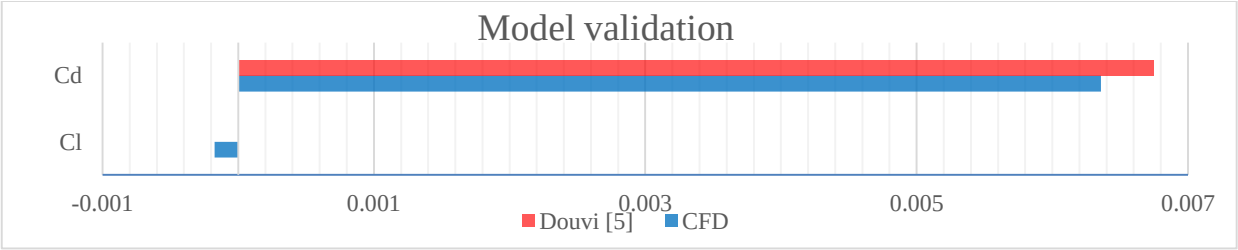

Fig. 10. Airfoil model validation

Car mesh test:

Car mesh is tested for solution independence using several mesh node resolutions and turbulence models, selected at three various speeds, 100kmph, 160kmph and 200kmph, which were chosen because they are realistic highway speeds.

The mesh test is conducted on a BMW E36 with a NACA 4412 inverted wing at an angle of attack of 14° as presented in Table 3.

 ISSN:Online 2790-1637, Print 2790-1629; National Library of Libya, Legal number : 154/2018

Table 3 BMW 3series (E36) mesh test

Nodes	180000	255927	355447	500000
Model	100kmph			
k kl ω	C_d	0.454195	0.450342	0.450922	0.448735
	C_l	-2.35805	-2.43034	-2.51799	-2.54053
	Drag (N)	422.6578	419.0728	419.6132	417.5776
	Lift (N)	-2194.32	-2261.59	-2343.16	-2364.13
	160kmph				Unstable
	C_d	0.43986	0.434905	0.435619	0.433068
	C_l	-2.37036	-2.40457	-2.45463	-2.4759
	Drag (N)	1047.853	1036.048	1037.75	1031.672
	Lift (N)	-5646.76	-5728.28	-5847.52	-5898.2
	200kmph				Unstable
	C_d	0.432401	0.470954	0.430603	0.428=059
	C_l	-2.32786	-2.55363	-2.40075	-2.41287
	Drag (n)	1609.508	1753.009	1602.813	1593.347
	Lift (n)	-8664.9	-9505.24	-8936.2	-8981.32
Spalart Allmaras	100kmph				
	C_d	0.432697	0.429656	0.428051	0.426511
	C_l	-3.56567	-3.54026	-3.58361	-3.55978
	Drag (N)	402.6533	399.8234	398.3297	396.8967
	Lift (N)	-3318.09	-3294.44	-3334.79	-3312.61
	160kmph				
	C_d	0.42761	0.42428	0.418946	0.418019
	C_l	-3.72755	-3.70285	-3.72101	-3.7048
	Drag (N)	1018.67	1010.739	998.0312	995.8191
	Lift (N)	-8879.92	-8821.09	-8864.35	-8825.73
	200kmph				
	C_d	0.425626	0.422212	0.41541	0.414556
	C_l	-3.80655	-3.78129	-3.79065	-3.77611
	Drag (N)	1584.29	1571.581	1546.265	1543.087
	Lift (N)	-14169	-14074.9	-14109.8	-14055.7
k-ω SST	100kmph				
	C_d	0.37115	0.357593	0.357179	0.358064
	C_l	-2.87933	-2.75098	-2.76362	-2.87303
	Drag (N)	345.3797	332.7639	332.3785	333.2018
	Lift (N)	-2679.4	-2559.97	-2571.73	-2673.54
	160kmph				
	C_d	0.353834	0.351034	0.350595	0.344617
	C_l	-2.92867	-2.90664	-2.91905	-3.00433
	Drag (N)	842.9171	836.2468	835.2017	820.9604
	Lift (N)	-6976.8	-6924.32	-6953.89	-7157.05
	200kmph				
	C_d	0.350211	0.348012	0.347617	0.34306
	C_l	-2.99511	-2.97821	-2.98996	-3.05896
	Drag (N)	1303.575	1295.39	1293.92	1276.959
	Lift (N)	-11148.6	-11085.7	-11129.4	-11386.3

 ISSN:Online 2790-1637, Print 2790-1629; National Library of Libya, Legal number : 154/2018

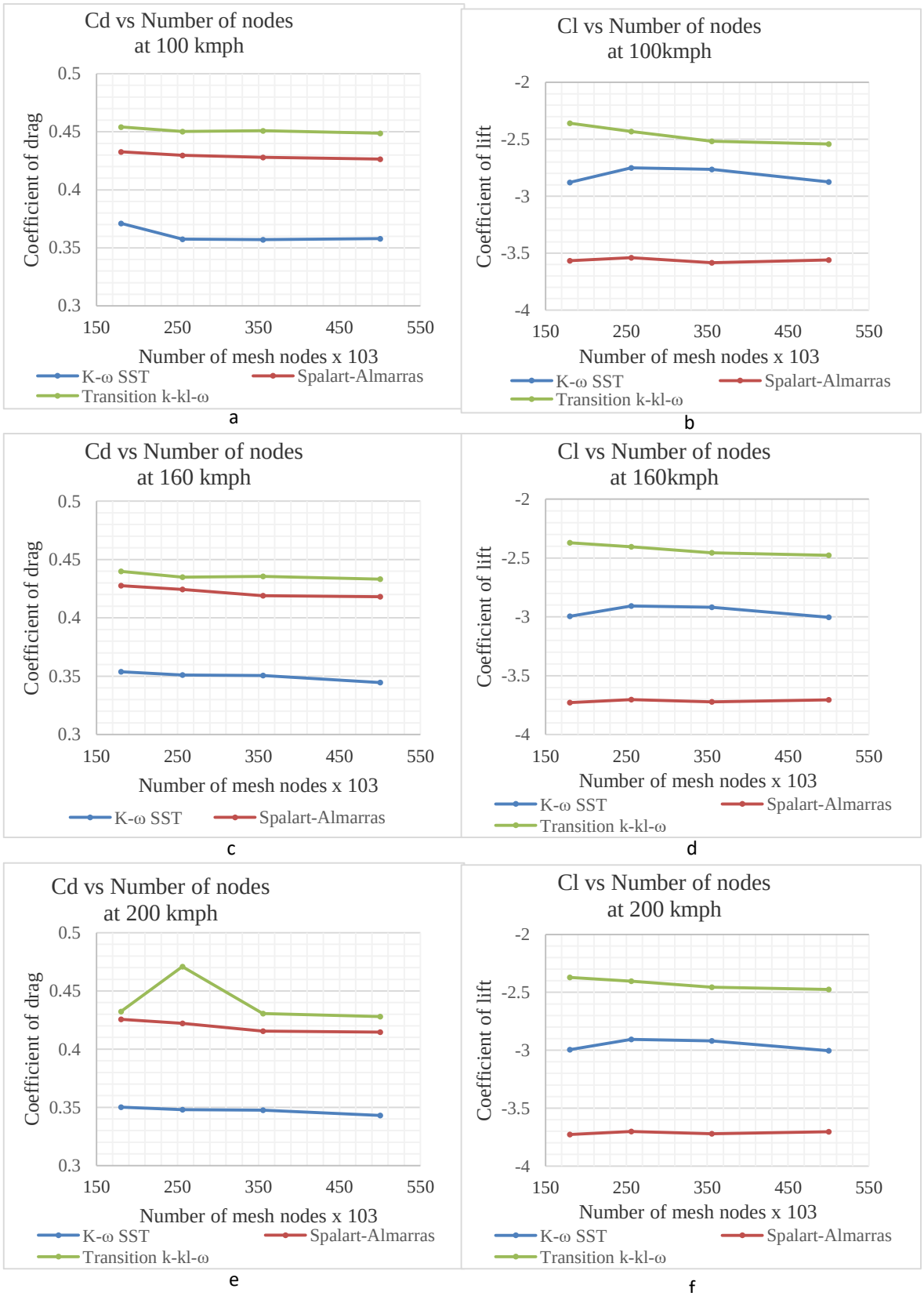

Fig. 11. a) Cd vs number of nodes at 100km/h b) Cl vs number of nodes at 100km/h c) Cd vs. number of nodes at 160km/h d) Cl vs number of nodes at 160km/h e) Cd vs number of nodes at 200km/h f) Cl vs number of nodes at 200km/h

 ISSN:Online 2790-1637, Print 2790-1629; National Library of Libya, Legal number : 154/2018

Table 4 BMW 3-series (E36) model validation

Spalart Allmaras	100kmph	
	C_d	0.254132
	C_l	-2.0065
	Drag (N)	236.4862
	Lift (N)	-1867.18
	160kmph	
	C_d	0.252933
	C_l	-0.99395
	Drag (N)	602.5467
	Lift (N)	-2367.82
	200kmph	
	C_d	0.249153
	C_l	-0.98211
	Drag (N)	927.4115
	Lift (N)	-3655.67

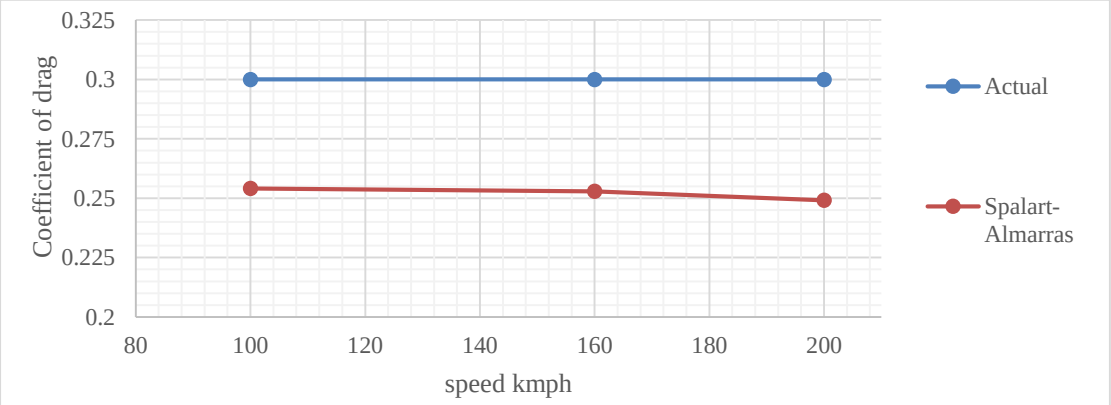

Fig. 12. BMW 3-series (E36) model

From the mesh independence test, it can be seen that the Spalart Allmaras has shown most stability from 355k node mesh to 500k node mesh, while the k-kl-ω transition model has shown instabilities and non-converged solutions in the 500k node mesh so it was eliminated, then the selected mesh was the 355k node with the Spalart Allmaras model, the selected mesh is to be validated.

The car simulation model was validated using actual results from BMW's service manual, the Cd is stated as 0.3 for the car, our 2D result for the same mesh for the car without any wing is around 0.25, with little change across different speeds, the error percentage is 16.67%, which is very reasonable since the 2D model doesn't account for wheels turbulence induced drag, side mirrors and other details that affect the drag, so it is reasonable for the drag to be less than the actual value.

3. RESULTS AND DISCUSSION

In this section, the results are presented and discussed thoroughly, simulations are divided into airfoils simulations and car with airfoil (inverted wing). The airfoils considered in the present work are: NACA 0012, NACA 4412 and Eppler E 423

Simulation of the airfoils:

In this stage of the simulation, the performance of three airfoils was compared using the selected and validated model in the previous section, the mesh test has shown that the best suited mesh for the selected

 ISSN:Online 2790-1637, Print 2790-1629; National Library of Libya, Legal number : 154/2018

conditions was the 355647-node mesh using the transition k-kl-ω turbulence model.

The angle of attack for all airfoils in freestream was chosen at 0 was to serve the objective of the study by highlighting the effect the difference in camber and shape of the airfoil had on its performance, as discussed in the mesh section earlier. It is worth to mention that Lift will be zero only for 0012, however, the study of the effect of angle of attack was not the objective of this study, it was to highlight the difference in performance of the airfoils in freestream and how it is reflected in the automotive application of the airfoil in an inverted rear wing.

The simulation conditions selected are:

Reynolds number = $3x10^6$, and AOA = 0^o

From equations 10 and 11, the Cd and Cl were calculated, and compared with experimental data (1)to evaluate the accuracy of the solution, the results are shown in Table 5, Figure 13 and Figure 14.

Table 5 Airfoil simulation results compared with experimental data

Airfoil		CFD results	Experimental results	Percentage error %
NACA 0012	Cd	0.00625686	0.00587	6.5%
	Cl	-0.000772	0	n/a
NACA 4412	Cd	0.006579026	0.006744	2.44%
	Cl	0.42086817	0.4129	1.9%
E 423	Cd	0.009057841	0.00915	1%
	Cl	1.1834935	1.16	2%

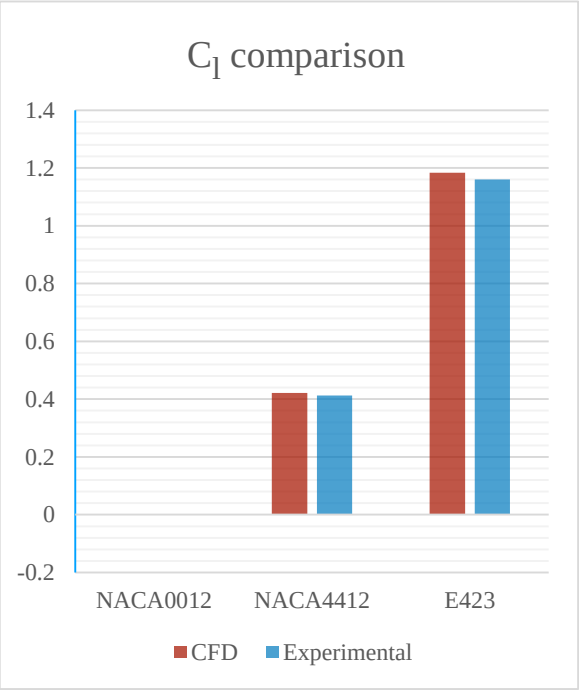

Fig. 13. Airfoil C_d comparison

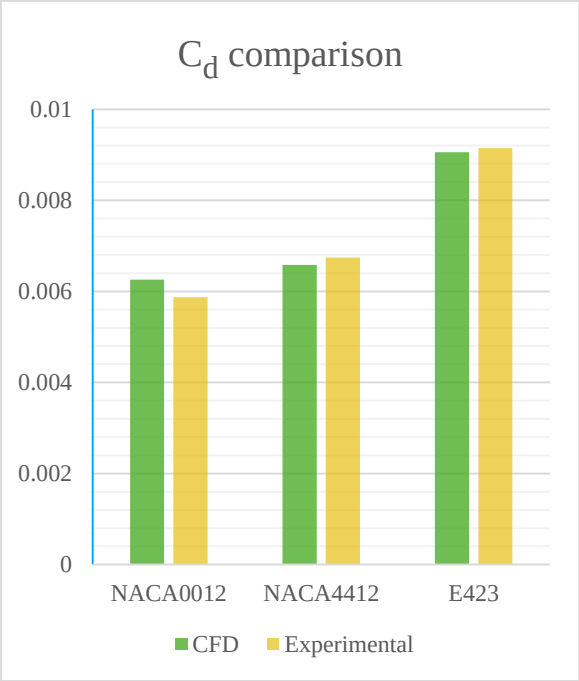

Fig. 14. Airfoil C_l comparison

 ISSN:Online 2790-1637, Print 2790-1629; National Library of Libya, Legal number : 154/2018

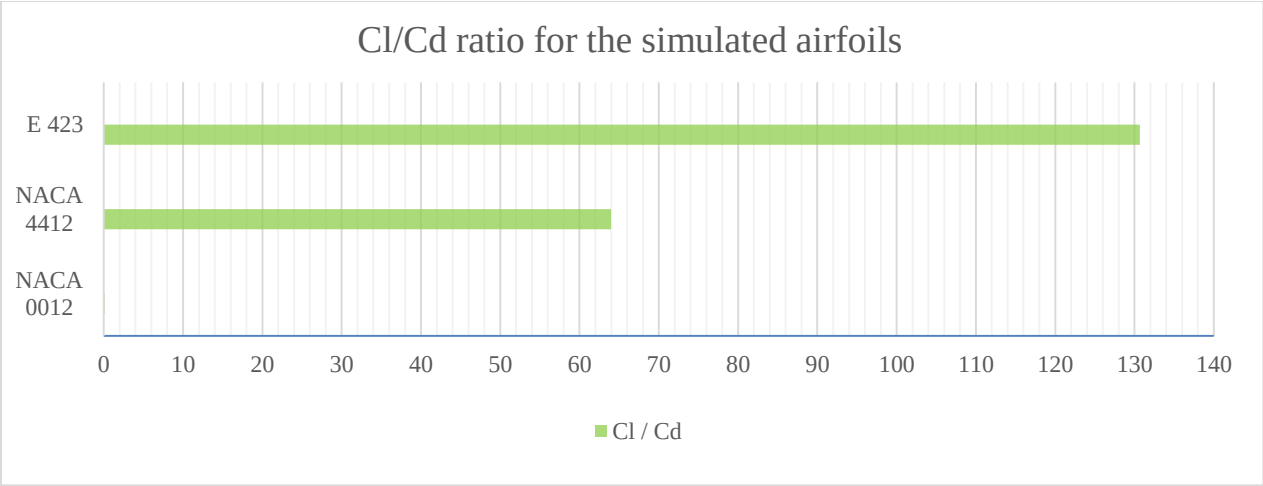

Fig. 15. C_l/C_d ratio for the simulated airfoils

The Cl value for the NACA0012 is very small that it can't be displayed in the graph. Given the favorable agreement displayed in the results, we proceeded with assessing the performance of each airfoil.

Table 6 C_l/C_d for airfoils

NACA 0012	0.12
NACA 4412	63.97
E 423	130.659

Table 6 and the Figure 15 show that at an AOA of 0^o the most lift to drag ratio was generated by the Eppler E423 airfoil, followed by NACA 4412, then NACA0012 generated almost no lift at all at an AOA of zero.

The performance of the airfoils will be further evaluated when used in an application in the second stage of the present study, in such a case where the automotive application as an inverted wing mounted on a BMW 3-series (E36).

Car simulation with airfoil (inverted wing):

In this section, the BMW 3 series (E36) was simulated without any modifications, using the selected mesh from the mesh test, with 355447 nodes and Spalart-Allmaras turbulence model, then the results were compared with actual C_d value in (25),a very good agreement was obtained, since the mesh is tested, one is now able to simulate the BMW 3-series (E36) with the modification of adding a rear inverted wing, the AOA of the airfoil is 14^o relative to the horizontal as discussed in the mesh section earlier.

Three different airfoils were used as inverted wings, to produce a negative lift force on the wheels, commonly known as downforce, to increase traction, increase max friction force and allow for faster acceleration without wheel spin, accordingly selection of the proper airfoil for the BMW is feasible.

The freestream velocities we used in the simulation are:

1. 100kmph (27.7778m/sec)
2. 160kmph (44.4444m/sec)
3. 200kmph (55.5555m/sec)

Just like the airfoil parameters calculated in the present of the study, equations 10 and 11, the Cd and Cl for the car's body was calculated and the results are shown in Table 7

 ISSN:Online 2790-1637, Print 2790-1629; National Library of Libya, Legal number : 154/2018

Table 7 BMW 3-series (E36)

	wingless	NACA4412	Eppler E423	NACA0012
100kmph				
Cd	0.254	0.429	0.435	0.4131
Cl	-2.003	-3.587	-3.8779726	-3.368
Drag (n)	236.47	400.14	404.79	384.42
Lift (n)	-1864.50	-3338.61	-3608.70	-3134.35
Moment at Rear wheel	2410.1392	3308.8741	3433.97	3200.92
160kmph				
Cd	0.249	0.419	0.429	0.407
Cl	-2.135	-3.719	-4.022	-3.514
Drag (n)	593.46	999.16	1022.20	969.859
Lift (n)	-5086.47	-8861.71	-9581.67	-8371.37
Moment at Rear wheel	6497.10	8812.37	9164.86	8562.57
200kmph				
Cd	0.247	0.415	0.426	0.404
Cl	-2.203	-3.789	-4.095	-3.588
Drag (n)	920.47264	1546.8291	1588.67	1505.96
Lift (n)	-8203.3524	-14103.952	-15245.31	-13355.38
Moment at Rear wheel	10408.47	14037.41	14607.09	13660.59

Table 7 and the graphs in figures 16 and 17 show that incorporating of the rear wing Eppler E423 exhibited the highest amount of lift force, moreover the highest drag force, followed by the NACA4412, then the NACA0012, it showed the lowest values for lift and drag.All wing modifications showed lift improvements over the unmodified BMW 3-series (E36), although lift improved as negative lift increase, it came with the penalty of drag forces increase, the evaluation for the best performance that can be gained from the wings which will be discussed next.

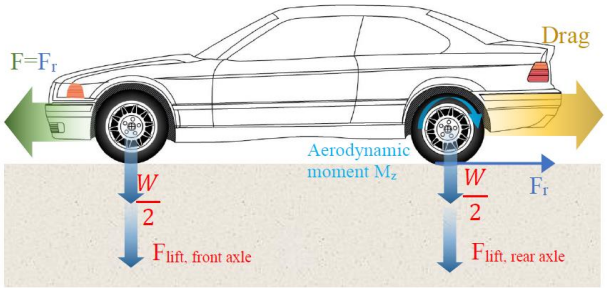

Fig. 16 BMW E36 force and moment analysis

 ISSN:Online 2790-1637, Print 2790-1629; National Library of Libya, Legal number : 154/2018

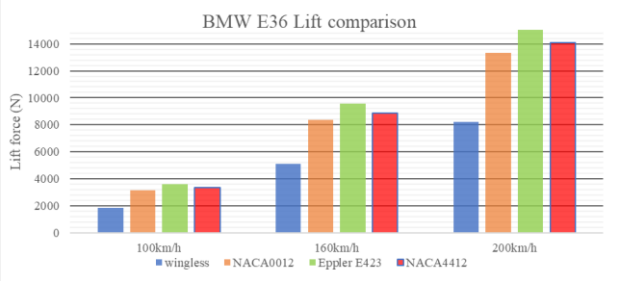

Fig. 17. BMW E36 Lift comparison

Table 7also presents the aerodynamic moment around the center of the rear wheels due to aerodynamic forces as shown in Figure 16 above, this moment is profound to evaluate the aerodynamic balance of the car, and will aid in the calculation of the maximum acceleration attainable using the force pushing down on the rear wheels, since the car in the current study is rear wheel driven.

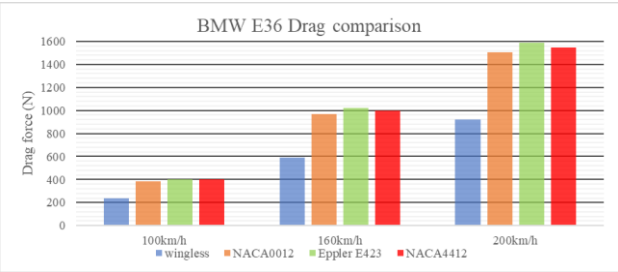

Fig. 18. BMW E36 Drag comparison

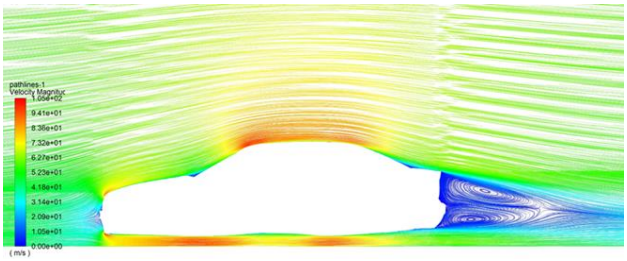

Fig. 19. BMW E36 wingless velocity lines

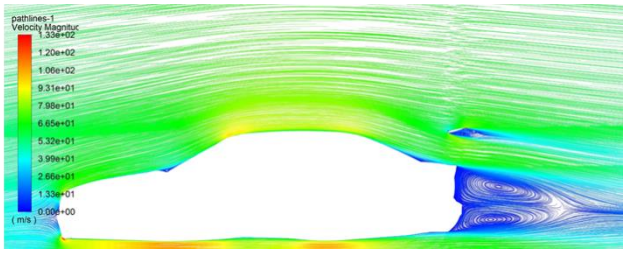

Fig. 20. BMW E36 with NACA0012 velocity lines

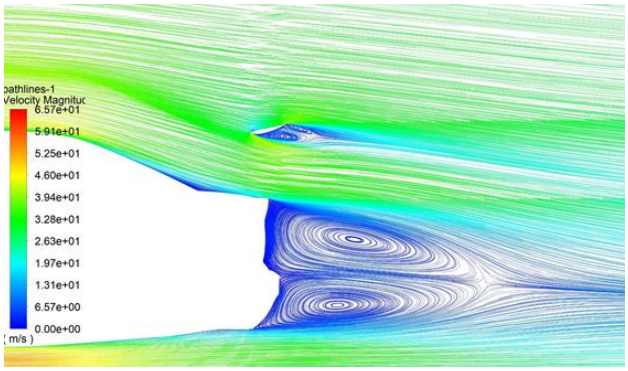

Fig. 21. BMW E36 with NACA4412 wing velocity lines wing

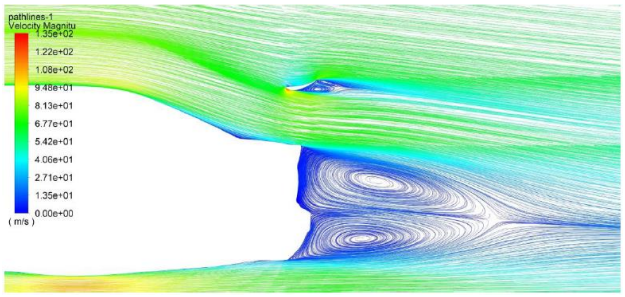

Fig. 22. BMW E36 with Eppler 423 wing velocity lines wing

Figures 19to22above depict the velocity lines for BMW E36 without and with the wings used in this study wing, the figures illustrate the characteristics of the flow for the BMW 3-series (E36) with the addition of the different airfoils as a rear wing and show the separation zone behind the car as well as behind the rear wing.

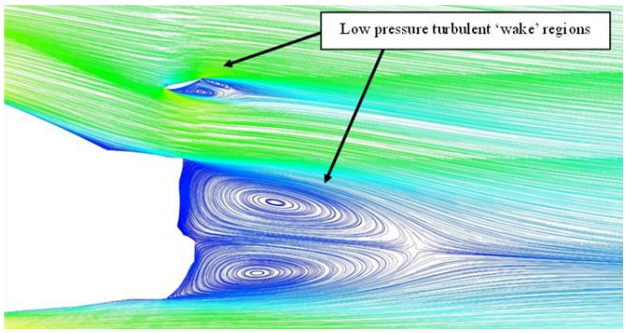

Fig. 23. Velocity Lines Showing Car Vortices and Low-Pressure Regions

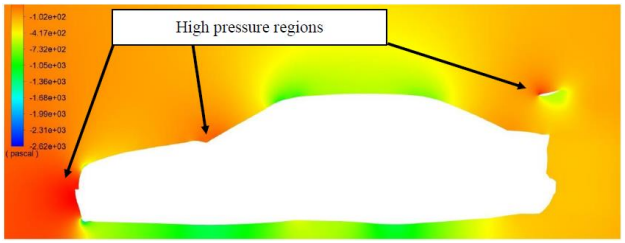

Fig. 24. Velocity Lines Showing Car Vortices and Low-Pressure Regions

 ISSN:Online 2790-1637, Print 2790-1629; National Library of Libya, Legal number : 154/2018

The velocity lines and pressure contour depicted in the figures 23 and 24 above respectively reveal an intriguing phenomenon: how the car produces drag and lift forces, and the role of the rear inverted wing in augmenting the negative lift force, known as downforce. The pressure contours indicate that the front end of the car experiences high pressure, while pressure decreases behind it, leading to drag that opposes the car's forward motion through the air. This relationship is confirmed by the velocity lines, as pressure and velocity are inversely related. The wake area formed behind the car, where separation occurs, creates a vacuum effect that draws in air at high speeds, resulting in low pressure behind the car. Figure 23 highlights these low-pressure regions.

4. CONCLUSION

The present sudy focused on the analysis of performnce of various aerfoils and testing them in a rear wing car in a numerical study, the following findings were highlighted as:

- The NACA 0012 produced the least due to it being a symmetrical aifoil, it produced the least amount of lift making it less suitable for applications requiring significant lift. In contrast, the NACA 4412 generates higher lift and drag forces. Conversely, the Eppler E423 produces the highest lift and drag forces due to its highly cambered shape, which creates a substantial pressure differential between the upper and lower surfaces of the airfoil.
- employing the airfoil in an automotive application as an inverted wing on a BMW 3-series (E36) car, the results indicate that at a specified angle of attack (AOA) of 14 degrees for the three airfoils, the NACA0012 exhibits the lowest drag and lift forces among them. Conversely, the Eppler E423 demonstrates the highest lift-to-drag ratio. However, it's important to note that this ratio alone does not necessarily guarantee the best performance. The evaluation of performance was conducted according to predetermined criteria
- The NACA4412 has demonstrated relatively high lift and drag forces compared to both the NACA0012 and the unmodified car without wings, although these values are not as high as those produced by the Eppler E423 airfoil.
- The conclusion drawn was that the Eppler E423 inverted wing demonstrated the best performance in terms of acceleration. It exhibited the greatest increase in potential acceleration that could be applied at the wheels without causing wheel spin or power loss. However, the NACA4412 closely followed suit, showing performance very similar to the Eppler E423. Conversely, the NACA0012 performed the worst in terms of acceleration potential. Nevertheless, it's noteworthy that all airfoils provided a performance advantage over the unmodified, wingless car body.
- After thorough consideration of the studied case, which includes the car model, the airfoils utilized, and the analyzed conditions and speeds, it is concluded that incorporating the Eppler E423 airfoil as an inverted wing onto the rear of the BMW 3-series (E36) car at an angle of attack of 14 degrees represents the optimal choice in terms of achieving both performance enhancements and safety improvements.

Nonetheless, future studies should meticulously evaluate the trade-offs between drag forces, associated power consumption, and the resulting performance gains to ensure a net positive impact on overall vehicle efficiency.

ACKNOWLEDGMENT

We acknowledge the collaborative spirit and commitment of our team members, whose collective effort made this work possible. While this research was conducted without external funding, the encouragement and support from our colleagues were influential in our research.

5. REFERENCES

1. Douvi EC, Tsavalos AI, Margaris DP. cfd calculations of the flow over a naca0012 airfoil. Momentum. 2010; 10:4.
2. Kevadiya M, Vaidya H. 2D analysis of NACA 4412 airfoil. Education. 2011;2013.
3. Reza MMS, Mahmood SA, Iqbal A, editors. Performance analysis and comparison of high lift airfoil for low speed unmanned aerial vehicle. International Conference on Mechanical, Industrial and Energy Engineering; 2016.
4. Panchal K. Computational Assessment of Front and Rear Wing of Amity Racing Vehicle. SAE Technical Paper, 2015 0148-7191.
5. Ahmed T, Amin MT, Islam SR, Ahmed S. Computational study of flow around a NACA 0012 wing flapped at different flap angles with varying Mach numbers. Glob J Res Eng. 2014;13(4):4-16.
6. Abobaker M, Elfaghi AM, Addeep S. Numerical Study of Wind-Tunnel Wall Effects on Lift and Drag Characteristics of NACA 0012 Airfoil. CFD Letters. 2020;12(11):72-82.
7. Bhatia D, Zhao Y, Yadav D, Wang J. Drag reduction using biomimetic sharkskin denticles. Engineering, Technology and Applied Science Research. 2021;11(5):7665-72.
8. Etaig SAM. Computation of Turbulent Buoyancy-affected Flows Relevant to Nuclear Reactor Cooling Applications: University of Manchester; 2007.
9. Sogukpinar H, editor the effects of NACA 0012 airfoil modification on aerodynamic performance improvement and obtaining high lift coefficient and post-stall airfoil. AIP conference proceedings; 2018: AIP Publishing.

 ISSN:Online 2790-1637, Print 2790-1629; National Library of Libya, Legal number : 154/2018

10. Karim MM, Prasad B, Rahman N. Numerical simulation of free surface water wave for the flow around NACA 0015 hydrofoil using the volume of fluid (VOF) method. Ocean engineering. 2014; 78:89-94.

11. Azim R, Hasan M, Ali M. Numerical investigation on the delay of boundary layer separation by suction for NACA 4412. Procedia Engineering. 2015; 105:329-34.

12. Hossain S, Raiyan MF, Akanda MNU, Jony NH. A comparative flow analysis of NACA 6409 and NACA 4412 aerofoil. International Journal of Research in Engineering and Technology. 2014;3(10):342-50.

13. Singh J, Singh J, Singh A, Rana A, Dahiya A. Study of NACA 4412 and Selig 1223 airfoils through computational fluid dynamics. SSRG International Journal of Mechanical Engineering (SSRG-IJME)–volume. 2015;2(6):17-21.

14. Saraf AK, Singh M, Kumar A. Analysis of the Spalart-Allmaras and kmω standard models for the simulation of the flow over a National Advisory Committee for Aeronautics (NACA) 4412 airfoil. 2012.

15. Saraf A, Nazar FA, Singh SP. Analysis of the k-ϵ and k-ω standard models for the simulation of the flow over a National Advisory Committee for Aeronautics (NACA) 4412 airfoil International Journal of Scientific & Engineering Research. Iternational Journal of Scientific & Engineering Research. 2013;4(6).

16. Petinrin M, Onoja V. Computational study of aerodynamic flow over NACA 4412 airfoil. British Journal of Applied Science & Technology. 2017;21(3):1-11.

17. Win SY, Thianwiboon M. Parametric optimization of NACA 4412 airfoil in ground effect using full factorial design of experiment. Engineering Journal. 2021;25(12):9-19.

18. <BOUANCY DRIVEN.pdf>.

19. Qu Q, Jia X, Wang W, Liu P, Agarwal RK. Numerical study of the aerodynamics of a NACA 4412 airfoil in dynamic ground effect. Aerospace Science and Technology. 2014; 38:56-63.

20. Huminic A, Huminic G. Automotive wing with active control of flow. UPB Scientific Bulletin, Series D: Mechanical Engineering. 2014;76(4):231-8.

21. Bhatkar O, Prabhutendolkar N, Sakpal A, Sawant S, Sakpal O. '2D analysis of multi-element airfoil for wing. International Research Journal of Engineering and Technology. 2018;5(2):174-7.

22. Sreejith B, Sathyabhama A. Numerical study on effect of boundary layer trips on aerodynamic performance of E216 airfoil. Engineering science and technology, an international journal. 2018;21(1):77-88.

23. Guda NT, Surisetti BV, Kolla SRC, Vasamsetti S. Enhancing Aerodynamic Performance of a Hatch Back Model Passenger Car using Ansys Fluent Software.

24. Kumar VN, Narayan KL, Rao L, Ram YS, Kumar V. Investigation of Drag and Lift Forces over the Profile of Car with Rear spoiler using CFD. International journal of advances in scientific research. 2015;1(08):331-9.

25. Kiley D. Driven: inside BMW, the most admired car company in the world: John Wiley & Sons; 2004.

 ISSN:Online **2790-1637**, Print **2790-1629**; National Library of Libya, Legal number : **154/2018**